JJEES

JJEES (2024) 15 (4): 257-264
ISSN 1995-6681

Jordan Journal of Earth and Environmental Sciences

Combined Geophysical and Soil Test Analysis Methods for Soil Precision Mapping in The Delta State University, Centre for Entrepreneurial Studies (CES) Farm, Abraka, Nigeria

Merrious Oviri Ofomola*[1], Ezekiel Onoriode Abriku[1], Bright Saturday Utieyin[2], Precious Okeoghene Otheremu[3], Ochuko Anomohanran[1]

[1]Department of Physics Delta State University Abraka, Delta State Nigeria
[2]Department of Science Laboratory Technology, Delta State Polytechnic, Otefe-Oghara, Delta State Nigeria
[3]Department of Physics, Delta State University of Science and Technology Ozoro, Delta State Nigeria

Received on August 1, 2024; Accepted on October 2, 2024

Abstract

Geophysical methods and soil test analysis have been used to study soil properties in the farm of the Centre for Entrepreneurial Studies (CES), Delta State University, Abraka, Nigeria. Vertical electrical sounding (VES), borehole geophysics, electrical resistivity tomography (ERT), and geochemical methods were used for the study. Seven VES stations were occupied along five traverses used for ERT measurements. Samples of soil close to the VES stations were taken for soil testing and to study their grain size to corroborate the results of VES and ERT. The low resistivity of the topsoil obtained from the VES agrees with the ERT and borehole log results and this ranges from fine-grained silt topsoil to sandy clay. This is a product of the partial decomposition of plants and animals forming organic matter. It ranges from 168 – 790 Ω.m with a mean value of 494 Ωm and an average depth of 2.3 m. This depth covers the upper root region of some important crops and depicts a high amount of moisture and mineral nutrients, and a fair degree of stoniness to aid adequate rooting of the crops. Also, the observed topsoil is high in porosity and water retention which are major suitable factors for the yield of tuber and stem plants. The soil test results are pH: 6.13-7.16, organic matter: 6.48-8.66 %, Nitrogen: 65.72-78.21 %, Phosphorus: 53.32-67.43 %, Copper: 14.16-22.61 mg/kg, Nickel: 1.16-3.11 mg/kg, Lead: 4.00-8.84 mg/kg, Arsenic: 0.08-0.1 mg/kg Iron: 96.33-151.63 mg/kg. These recorded concentrations are below the WHO standard for crop production.

Keywords: *Precision Agriculture, Crop Yield, Soil Test, Contamination Factor, Organic Matter*

1. Introduction

Agricultural production is declining due to soil degradation, poor soil biology, lower yield, stunted plant growth, and water erosion. Soil quality is important for agriculture, forestry, and environmental protection, but traditional methods of assessing soil can be costly and time-consuming. Properties of soil which include organic and mineral content, soil solution, and salinity are essential for precise agriculture. Soil organic matter composition is the summation of plants' and animals' remains. It provides a totality of nutrients and moisture to the soil which, in turn, reduces contraction and aids water infiltration into the soil. The soil volume is mostly consisting of stones, sand, silt, and clay. The decomposition rate is slow for soil and rich in clay, shale, and silt. This decomposition releases fewer nutrients as compared to sandy soil which will cause an improved breakdown and deployment of biological materials into the ground (Romero-Ruiz et al., 2018). Therefore, soil, rich in clay, shale, and silt, will cause a reduction in the electrical resistance of the surface soil. Soil, heavy with metal contamination, is a major concern for farming, as it can negatively affect crop growth and human health. Heavy metal contamination of the soil is a major factor, contributing to soil pollution (Anomohanran 2015; Iserhien-Emekeme et al., 2021; Ofomola et al., 2021; Rashid et al., 2023). Heavy metals, such as Fe, Zn, Ca, and Mg, are vital for human health, whereas As, Cd, Pb, and methylated classes of mercury can be dangerous even at low doses. Heavy metals have harmful effects on soil microbial communities. They can alter soil production and hinder essential plant activities (Briffa et al., 2020; Saikat et al., 2022; Mashal et al., 2017; Lu et al., 2014). Metals, absorbed by plants from soil, pose a significant health danger to the food chain. Traditional soil analysis methods involve chemical digestion, and they are time-consuming and expensive. These techniques are promising for on-site analysis of heavy metal levels in soil, which can help farmers make informed decisions regarding soil management practices. One advantage of Graphite Furnace Atomic Absorption Spectroscopy (GFAAS) over other soil analysis methods is its sensitivity and ability to detect trace amounts of elements in soil samples (Nowka et al., 1999; Ofomola, 2015; Aweto et al., 2017; Altunay et al., 2021; Liu et al., 2023). GFAAS can detect heavy metals like lead, cadmium, arsenic, and mercury in soil at concentrations as low as parts per billion (ppb), making it a highly sensitive analytical tool for environmental monitoring and research purposes. Additionally, GFAAS is a simple, fast, and precise method that requires minimal sample preparation, making it

* Corresponding author e-mail: ofomola@delsu.edu.ng

a cost-effective and efficient technique for analyzing large numbers of soil samples. GFAAS offers higher sensitivity and precision than other methods for trace element analysis in soil, allowing the detection of heavy metals at concentrations as low as parts per billion. The moisture level in the soil is vital for crop growth as it significantly impacts key physiological functions of plants, including water absorption, nutrient distribution, photosynthesis, temperature control, cell enlargement, growth, and resilience to stress. Soil moisture refers to the level of wetness in the top layer of soil relative to its ability to hold water, which is influenced by factors like precipitation, evaporation, temperature, and the properties of the soil itself. The soil moisture index (SMI), a scale without units, quantifies the moisture content of the soil and is crucial for various environmental aspects, such as agriculture and water resource management. Modern remote sensing methods have improved and refined assessments, making them more efficient for tracking indicators like soil moisture index (SMI), land surface temperature (LST), and the Normalized Difference Vegetation Index (NDVI) (Carlson et al., 1994; Ali et al., 2022). These techniques offer quick and ongoing evaluations of surface-level moisture across extensive regions. LST calculations are derived from thermal emissions, whereas NDVI measurements are based on specific segments in the realm of the electromagnetic spectrum, particularly the reflectivity on the surface within the red and near-infrared (NIR) bands. Geophysical techniques allow for fast and non-disturbing measurement of soil characteristics, like electrical conductivity, resistivity, and potential methods, making them an efficient approach for precise agriculture mapping (Ozegin and Safulu, 2022; Ganiyu et al., 2020). Electrical resistivity is vital for soil mapping and investigations, depending on the approach utilized, which can be 1D, 2D, or 3D. Aided by this technique, the near-surface zone's vertical and lateral variability can be evaluated. Electrical resistivity can be applied to agricultural areas to characterize soil factors, such as soil texture, wetness, and salinity, as well as heavy metal pollution (Turki, et al., 2019; Vásconez-Maza, et al., 2021). The outcomes of this study will establish the possibility of measuring soil salinity, soil moisture, and soil texture from geophysical methods. High salinity regions are simply distinguished with electrical resistivity, and the soil layering is marked to a depth of about 2 m, being the interval encompassing both the soil profile and the precinct where crop roots thrive (Allred et al., 2008).

Therefore, this study aimed at applying both geophysical and geochemical principles for soil mapping and characterization in the context of sustainable precise farming practices in the Centre for Entrepreneurship Study (CES) farm, Delta State University, Abraka, Delta State, Nigeria.

2.1 Materials and Methods

2.1.1 Site Description and Geology

Abraka is situated in the Western Niger Delta within latitudes 50° 48" N and longitude 60° 06" E (Figure 1), and underlying the area is the Benin Formation, extending over the River Niger with a stretch covering the west of Lagos and extending to the Calabar Flank. It has a lowland terrain typical of a coastal plain, sloping towards the River Ethiope. The climate and relative humidity range from 23 to 37°C and 50 to 70%, respectively. Also, the annual dry and wet periods are from about November to February, and March to October, respectively. Between 2000-2005, the Delta State University weather station measured the mean rainfall in the area to be 3317.8 mm. Abraka has rainforest vegetation that has been converted to farmlands and ancillary forests. However, the riverbanks are flanked by lush, dense, and swamp primary forest. Three lithostratigraphic formations make up the Geology of the area: The Akata Formation, Agbada Formation, and Benin Formation. They constitute the geological landscape, along with the Akata being the oldest and Benin the youngest. The Benin Formation is obscured by the newer Holocene sediments found in the Sombreiro-Warri Deltaic plain, as well as the Mangrove swamp and freshwater swamp wetlands located in the south of Abraka. (Ofomola et al., 2018). Thestudy area is the CES farm at Site III of the Delta State University,Abraka (Figure 2), situated in the northeastern part of Isiokolo. It has existed for about 7 years with various crops such as pineapple, cassava, banana, yam, and watermelon, cultivated on the farm.

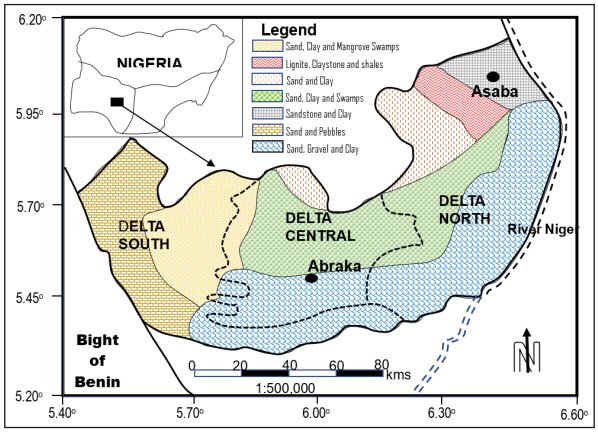

Figure 1. Geological map of Delta State showing the study area

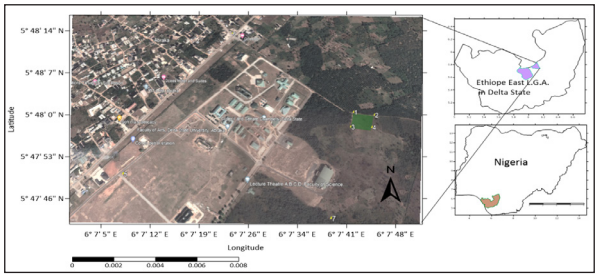

Figure 2. Location map of DELSU showing the study area

2.2 Elctrical Resistivity Method

An electrical resistivity survey, which employed vertical electrical sounding (VES) and two-dimensional (2D) resistivity mapping was performed at the location, utilizing the ABEM Tetrameter (SAS 1000) to map the subsurface lithology and characterisation of the topsoil. The base map for the electrical survey is presented in Figure 3. A total of seven VES and five - 2D-ERT profiles were occupied using Schlumberger and modified Wenner arrays, respectively.

The Win-Resist program, Version 1.0 (Vander-Velpen, 2004) was used to produce a resistivity model of one-dimension (1D) for each sounding location. The graphs display the estimated resistivity, thicknesses, and depths of

the geoelectric strata at every VES station (Aizebeokhai, 2010).

An extended profile dimension of 100 m with the least possible electrode spacing and increment of 1 m was chosen for each 2D traverse line while using the modified Wenner electrode array setup for 5 data levels. The values of the apparent resistivity from the ERT were processed, using RES2DINV inversion software, version 3.59 (Loke 2010) to produce the inverse model resistivity, which aided in the understanding of the subsurface distribution of resistivity (Ofomola et al., 2016; Al-Amoush et al., 2017; Chinyem 2024). The program subdivides the area under the surface into a series of rectangular zones that reflect the observed data layout. The traditional Least-square approach was utilized to process the 2D data in a bid to reduce to barest. It minimizes the squared discrepancies of the variance between the actual and modeled apparent resistivity readings.

Figure 3. Base map consisting of lines and designated sampling points at the CES farm

2.3 Geochemical Method

Soil samples were collected at seven different sample points, close to the VES stations, for critical examination and analysis at the Advanced Research Laboratory of Delta State University, Abraka. This will validate the resistivity values obtained in the area (Ofomola et al., 2021). To obtain the soil in its pristine condition free from environmental contamination, samples were taken from a depth of 0.5 meters without any disruption and were promptly stored in airtight sampling bags. The soil samples were analyzed for heavy metals and rare earth elements (REE) such as copper (Cu), cobalt (Co), lead (Pb), zinc (Zn), nickel (Ni), molybdenum (Mo), cadmium (Cd), arsenic (As), using the Graphite Furnace Atomic Absorption Spectrophotometer (GFAAS). Li et al. (2017) identified this as one of the top techniques for quantifying heavy metals and REE in soils. The heavy metals are reported in ppm, whereas the concentration is given in %. One ppm is equal to one mg/kg when converting from ppm to mg/kg. Additionally, 1 g/kg = 0.001 ppm since 1 g/L or 1 g/kg equals 1 ppb, which is identical to 1 ppb.

Determination of contamination level was conducted using the contamination factor (Cf) and the pollution load index (PLI), (Tomlinson et al., 1980), where the Cf was derived using Eq. (1).

$$Cf = \frac{\mathrm{Cn}}{Bn} \quad (1)$$

Cn is the metal concentration level, and Bn represents the baseline or average crustal elements value. A Cf (contamination factor) of up to 1 depicts low contamination, a Cf extending from more than 1 to 3 indicates moderate contamination, and a Cf above 3 means high contamination levels. Earlier studies utilized the pollution load index (PLI), alternatively recognized as Tomlinson's pollution index, and the Nemerow integrated pollution load index (NIPI) to evaluate the comprehensive pollution condition of soil specimens. (Nemerow, 1991; Tomlinson et al., 1980). The PLI was calculated using Eq. (2)

$$PLI = \sqrt[n]{cf1 \times cf2 \ldots . cfn} \quad (2)$$

where the pollution load index, PLI is determined by the number of samples, n, and contamination factor of metal n, . The PLI index runs through a scale ranging from 0 to 6, where 0 indicates no pollution, 1 signifies pollution from none to medium, 2 denotes moderate pollution, 3 is an indication of moderate to strong pollution, 4 signifies strong pollution, 5 represents pollution status from strong to very strong, and 6 signifies very strong pollution, as highlighted in studies by Finch et al. (2018), and Rashed (2010).

2.4 Soil Moisture Estimation using Landsat Image

The analysis of the Soil Moisture Index (SMI) was carried out using Landsat 8 imagery at a resolution of 30 meters, which had minimal cloud interference and was sourced from the United State Geological Survey (USGS) Earth Explorer website. The SMI analysis and mapping were executed using the raster calculator tool in ArcGIS 10.2.2, a geographic information system software. SMI maps, created using Landsat 8 images, display values ranging from 0 to 1, which indicate the comparative volume of soil moisture present in the area. On these maps, a value of 0 indicates the least amount of soil moisture, whereas a value of 1 signifies the maximum soil moisture observed on a specific day.

The computation of the SMI entailed incorporating the Normalized Difference Vegetation Index (NDVI) with the Land Surface Temperature (LST), a method used by Ijaz et al. (2020) and Tajudin et al. (2021). The SMI was determined using the formula in Eq. (3)

$$\mathrm{SMI} = (\mathrm{LST}_{max} - \mathrm{LST}) / (\mathrm{LST}_{max} - \mathrm{LST}_{min}) \quad (3)$$

where, for a specific NDVI, $\mathrm{LST}_{max,}$ and LST_{min} represent the highest and lowest surface temperatures, respectively, and LST refers to the surface temperature of a pixel for that NDVI, as measured through remote sensing. NDVI values, which can vary from -1 to 1, are calculated using Eq. (4)

$$NDVI = (NIR - Red) / (NIR + Red) \quad (4)$$

where NIR and Red represents the Near-infrared band and Red band, respectively.

3.1 Results and Discussion

3.1.1 Geoelectrical Resistivity Methods for Soil Profile Delineation

The results of resistivity sounding revealed inferred lithology, layer thicknesses, and depths as shown in Table 1. A geoelectric section, utilizing the borehole log information alongside vertical electrical sounding data, was constructed as shown in Figure 4. The geoelectric sections and the borehole log, upon comparison, show similar content but vary in the structure and depth associated with various soil types.

Table 1. Geoelectric parameters and related lithology

VES	LAYERS	RESISTIVITY (ohm.m)	THICKNESS (m)	DEPTH (m)	INFERRED LITHOLOGY
1	1 2 3 4 5	168.3 1942.9 2702.8 3040.1 3321.2	1.0 7.9 31.4 8.0	1.0 8.9 40.3 48.3	Lateritic Topsoil Fine sand Fine to medium-grain sand Medium to coarse sand Coarse sand
2	1 2 3 4 5	224.6 4207.9 3939.2 2965.7 3317.1	0.8 3.6 10.0 11.0	0.8 4.4 14.4 25.4	Lateritic Topsoil Sand Fine sand Fine to medium-grain sand Coarse sand
3	1 2 3	624 2674 3526	1.7 13.2	1.7 14.9	Lateritic Topsoil Fine to medium-grain sand Coarse sand
4	1 2 3 4	528 4557 2500 3695	1.5 3.6 13.5	1.5 5.1 18.6	Topsoil Fine sand Fine to medium-grain sand Coarse sand
5	1 2 3 4	790 2551 1795 2248	1.2 3.5 14.5	1.2 4.7 19.2	Lateritic Topsoil Fine sand Fine to medium-grain sand Coarse sand
6	1 2 3	597 2908 1120	0.7 3.7	0.7 4.4	Lateritic Topsoil Fine sand Coarse sand
7	1 2 3 4	523 397 2276 1628	3.1 5.2 24.2	3.1 8.3 32.5	Lateritic Topsoil Fine sand Fine to medium-grain sand Coarse sand

The outcomes of vertical electrical sounding (VES) tests, provided in Table 1, show the inferred lithology and associated resistivity and depth of different strata.

The first VES location (VES 1) has five layers, with resistivity ranging from 168.3 Ωm for the lateritic topsoil layer to 3321.2 Ωm for the coarse sand layer. The layer thicknesses range from 1.0 to 31.4 m. The inferred lithology includes topsoil, fine sand, fine to medium grain sand, medium to coarse sand and coarse sand. VES 2 also has five layers, with resistivity ranging from 224.6 Ωm for the lateritic topsoil layer to 4207.9 Ωm for the sand layer. The layers' thicknesses range from 0.8 m to 11.0 m. The inferred lithology includes lateritic topsoil, sand, fine sand, fine to medium-grain sand, and coarse sand. VES 3 has three layers, with resistivity ranging from 624 Ωm for the lateritic topsoil layer to 3526 Ωm for the coarse sand layer. The thickness of the layer ranges from 1.7 m to 13.2 m. The inferred lithology includes topsoil, fine to medium-grain sand and coarse sand.

The fourth VES location (VES 4) has four layers, with resistivity ranging from 528 Ωm for the lateritic topsoil layer to 4557 Ωm for the fine sand layer. The thickness of the layers ranges from 1.5 m to 13.5 m. The inferred lithology includes topsoil, fine sand, fine to medium-grain sand, and coarse sand. The fifth VES location (VES 5) has four layers, with resistivity ranging from 790 Ωm for the lateritic topsoil layer to 2551 Ωm for the fine sand layer. The thickness of the layer ranges from 1.2 m to 14.5 m. The inferred lithology includes lateritic topsoil, fine sand, fine to medium-grain sand, and coarse sand. VES 6 has three layers, with resistivity ranging from 597 Ωm for the topsoil layer to 2908 Ωm for the fine sand layer. The thickness of the layers ranges from 0.7 m to 3.7 m. The inferred lithology includes topsoil, fine sand and coarse sand. VES 7 has four layers, with resistivity ranging from 397 Ωm for the fine sand layer to 2276 Ωm for the fine to medium grain sand layer. The thickness of the layers ranges from 3.1 m to 24.2 m for the fine to medium-grain sand. The inferred lithology includes lateritic topsoil, fine sand, fine to medium-grain sand, and coarse sand.

Generally, the VES revealed three to five geoelectric layers across the study area. The near-surface first layer exhibits a resistivity range from 178-790 Ωm and a thickness of 0.7-3.1 m, and this mainly represents the lateritic topsoil. The second layer's resistivity and thickness vary from 397-4557 Ωm and 3.5-7.9 m, respectively, and are dominated by lateritic fine sand. The third to fifth layers constitute the saturated zone which is the basic source of moisture for the crops and has resistivity ranging 1120-3695 Ωm and thickness ranges 10.0- 31.4 m, and they represent the fine sand from medium to coarse grain sand.

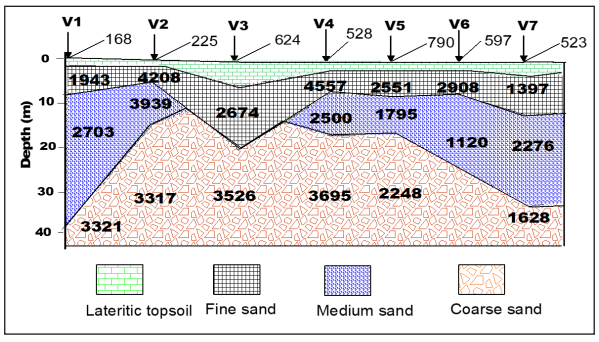

Figure 4. Geoelectric profile through VES 1 to VES 7.

3.1.2 Soil Profile Evaluation

To obtain the soil profile in the study area, borehole drilling data as well as the downhole geophysical logs were used as presented in Figure 5. The first layer consists of brownish, unconsolidated, lateritic topsoil of about 3 m thick. The dark brown coloration is due to the humus and organic matter content. This makes the soil to a depth of 3 m suitable for crop production. A reddish lateritic sand layer to a depth of 6.5 m underlain the first layer. From this lower portion, the values of resistivity and spontaneous potential logs are approximately 500 Ω. m and -0.4 mV, respectively, due to the degree of moisture. The third layer thickness is around 2.7 m, to a depth of 9.1 m, and is composed of reddish brown, fine clayey sand. Also, the composition of the fourth layer is brownish fine to medium sand, while the fifth layer is about 4.1 m thick, extending from a depth of 12.2 m - 16.3 m and is composed of brownish to yellowish fine to medium to coarse sand. The sixth layer has a depth range between 19.6 and 48.8 m and is composed of whitish, medium to coarse sand. The resistivity log shows an increase of 400 Ωm, while the SP log value shows a more stable value, indicating complete saturation.

This soil profile determination corresponds with the inferred lithology from the geoelectric section, obtained from the vertical electrical sounding which ranges from lateritic topsoil to saturated coarse sand. The resistivity of the topsoil ranges from 168 – 790 Ωm with an average value of 494 Ωm and an average depth of 2.3 m. This depth covers the uppermost root area of some significant crops such as maize, okra, cucumber, cassava, tomatoes, etc. The topsoil resistivity values depict a high amount of moisture and mineral nutrients, and they have a fair degree of stoniness to aid adequate rooting of the crops.

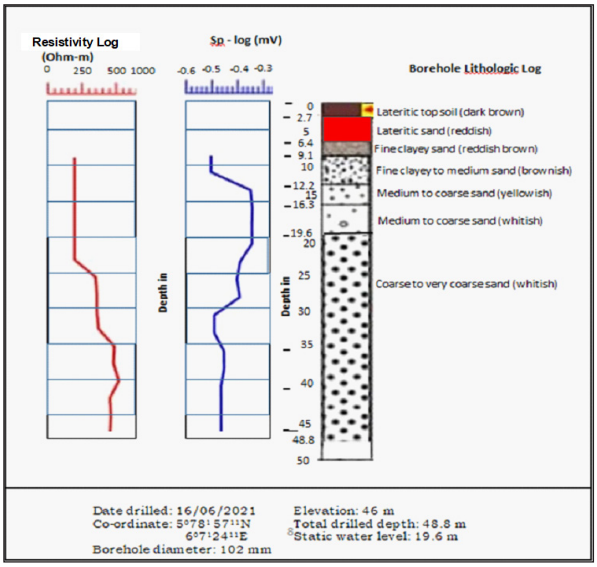

Figure 5. Cross section of the lithologic log from the borehole plotted against a downhole geophysical log in the area.

The 2D resistivity inversion models, including elevations for the traverses conducted on the CES farm, are presented in Figure 6. Six layers were identified, and they agree with the vertical electrical sounding and the borehole log. The 2D images have an approximate investigation depth of 3 m. The values, presented on the vertical edges of the sections, correspond to the elevations of each traverse line. The variation in resistivity values is a function of mineral and moisture contents and degree of compaction of the soil. The topsoil comprises lateritic clay and sandy clay with a resistivity of less than 300 Ωm and a depth of about 1.5 m. The variation in the soil compaction, moisture level, and content of organic matter is blamed for the shift in values of resistivity obtained across the traverses. Except for traverse 2, the topsoil, across the study area, is rich in moisture and mineral composition , similar to the assertion made by Ozegin and Salufu (2022). The low resistivity of fine-grained silt and clay topsoil is because of the partial decomposition of plants and animals forming organic matter. Also, the observed topsoil is high in porosity and water retention which are major suitable factors for the yield of tuber and stem plants. The second layer resistivity values greater than 600 Ωm are an indication of organic matter deficiency in the soil (Ozegin and Salufu, 2022). The soil stoniness has increased in this level, thereby reducing the effective rooting of crops and reducing the water retention capacity since the soil is now semi or non-permeable. The soil at this level also contains little or no organic matter due to the low presence of microorganisms, arising from the low water retention capacity (Verdoodt and Ranst, 2003). This is a major limitation to the crop yield capacity of the soil.

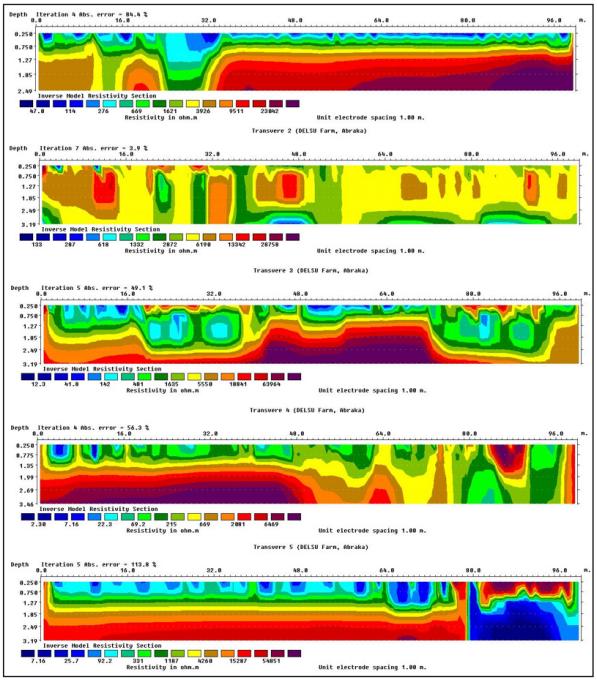

Figure 6. Results of inverted ERT profiles

3.2 Soil Analysis Results

Table 2 outlines the concentrations of major trace and rare earth elements in the soil samples collected from the study area. The pH ranges from 6.13 to 7.16 across the designated sample points in the study location. This falls within the acceptable range of 6.0 – 7.5 and indicates good soil for crop production. Organic matter content ranges from 6.48 – 8.66 % with stations 1, 2, 4, and 7 having a relatively high organic matter content. This result agrees with the VES, with topsoil of less than 600 Ωm, which is an indication that the soil exhibits moderate richness in mineral and natural organic content required for crop production (Ozegin and Salufu, 2022).

Table 2. Heavy metals detected from soil samples, compared with WHO/FAO permissible limits for heavy metals in soil.

Parameters	Crustal average (1964)	S1	S2	S3	S4	S5	S6	S7	WHO /FAO
pH	-	6.13	6.51	7.11	6.31	7.16	7.12	6.21	7.50
Organic matter (%)	-	8.37	8.21	`6.74	8.66	6.48	7.95	8.42	N/A
Total Nitrogen (%)	-	65.72	68.61	75.82	72.15	73.51	78.21	68.42	N/A
Phosphorus (mg/kg)	-	53.32	55.98	58.45	67.43	62.67	65.32	66.24	N/A
Cadmium (mg/kg)	0.1	0.06	0.08	0.02	0.10	0.11	0.04	0.07	0.8
Chromium (mg/kg)	83.0	3.10	1.47	1.31	0.42	0.56	0.19	0.59	100
Copper (mg/kg)	25.0	22.61	18.41	16.91	27.43	25.63	14.16	20.41	36
Nickel (mg/kg)	44.0	2.06	1.16	2.16	1.84	3.11	2.10	1.89	35
Lead (mg/kg)	17.0	7.46	4.86	6.11	5.11	8.84	3.67	4.00	85
Zinc (mg/kg)	71	1.09	1.17	0.98	2.16	2.94	1.81	1.94	60
Cobalt (mg/kg)	17.0	0.95	1.07	1.00	1.14	12.07	1.84	1.27	N/A
Manganese (mg/kg)	600	2.09	1.84	2.84	15.61	17.07	14.11	12.16	N/A
Iron (mg/kg)	N/A	98.41	103.41	96.33	149.11	151.63	131.63	120.74	300
Arsenic (mg/kg)	1.5	N/A	N/A	N/A	0.10	0.08	N/A	N/A	10

N/A: Means not Available.

Also, the values for total nitrogen and phosphorus range from 65.72 % - 78.21 %, and 53.32 – 67.43 mg/kg, respectively. Stations 3, 5, and 6 have lower organic matter content, with higher resistivity of the topsoil > 600 Ωm. This establishes that the area has low crop yield capacity with topsoil resistivity values, ranging from 597 – 790 Ωm. The soil nutrients spatial dissemination in the study area shows that the area around stations 1.2 4 and 7 is rich in essential soil nutrients while stations 3, 5, and 6 have low nutrients and are deficient of organic matter.

The concentration of copper (Cu) varied from 14.16 mg/kg to 22.61 mg/kg, which is under the WHO-allowed upper limit for agricultural soils of 40 mg/kg. Copper-induced toxicity is typically detected in the soil and water in industrialized areas. The concentration of nickel (Ni) ranged from 1.16 mg/kg to 3.11 mg/kg as shown in Table 2, which is also below the WHO/FAO acceptable threshold of 68 mg/kg for agricultural soils. As a micronutrient, Ni is fundamentally needed in tiny amounts for proper plant growth. However, when toxic levels are present in soil, it restricts plant development, stunts root growth, and induces chlorosis, which is characterized by the yellowing of leaves due to a lack of chlorophyll. The concentration of Lead (Pb) in the samples was between 4.00 mg/kg and 8.84 mg/kg, which falls under the acceptable threshold of 50.00 mg/kg set by WHO/FAO (2001) for agricultural soils. Arsenic (As) was not detected in the farm except in samples 4 and 5, the farm has concentrations ranging from 0.08 mg/kg to 0.1 mg/kg and are within the WHO/FAO acceptable limits of 10 mg/kg.

Also, Iron (Fe) content in the samples ranged between 96.33 mg/kg and 151.63 mg/kg. The impacts of iron (Fe), a vital micronutrient for agricultural soils, involve field yellowing and the formation of irregularly shaped regions in the subsurface. The maximum permitted content of Fe in soil, according to the WHO, is 450 mg/kg. However, the iron concentration in the CES farm is below the WHO-recommended levels. These observed concentrations render the soil at the CES farm of Delta State University free from toxicity and thereby suitable for crop production (WHO/FAO, 2001). The contamination factor and pollution index for the soil are presented in Table 3.

Table 3. Pollution index and contamination levels of the toxic elements of the soil

Toxic elements	Contamination Factor (Range)	Contamination Factor	Pollution load index (PLI)	Interpretation
Cadmium	0.2-1.1	0.69	0.60	Unpolluted
Chromium	0.0-0.04	0.01	0.01	Unpolluted
Copper	0.68-1.03	0.83	0.82	Unpolluted
Nickel	0.03-0.07	0.05	0.05	Unpolluted
Lead	0.24-0.52	0.34	0.07	Unpolluted
Zinc	0.01-0.04	0.02	0.02	Unpolluted
Cobalt	0.06-0.71	0.31	0.10	Unpolluted
Manganese	0.00-0.03	0.02	0.01	Unpolluted
Iron	N/A			Unpolluted
Arsenic	0.05-0.07			Unpolluted

The contamination factor (CF) from toxic elements of Cd, Cr, Cu, Ni, Pb, Zn, Co. Mg, and As range from 0.2 - 1.1, 0.0 - 0.04, 0.68 - 1.03, 0.03 - 0.07, 0.24 - 0.52, 0.01- 0.04, 0.06 - 0.71, 0.00-0.03 and 0.05 - 0.07, respectively. This is an indication of low to moderate contamination, low salinity, and high levels of organic material in the soil. Also, the soil

pollution load index (PLI) ranges from 0.01 - 0.82. This also indicates that the entire soil in the study area is unpolluted. The soil analysis results concur with the borehole log, VES, and electrical resistivity tomography, signifying that the soil is high in organic content.

Table 4 shows the textural analysis of the soil with silt having the dominant grain ranging from 66.2 % to 73.0 %, clay from 15.4 % to 19.4 %, and sand from 11.6 % to 16.1 %. Clay content is moderately high in the area which is an indication of the Cation Exchange Capacity (CEC) of the soil and retention of nutrients. Also, a combination of the clay and silt content increases moisture retention. These values are higher around locations 1. 2. 4 and 7 and in agreement with the soil nutrients analysis and the VES.

Table 4. Soil textural analysis results in the CES Farm

Sample	Silt (%)	Sand (%)	Clay (%)
S1	72.3	12.2	16.5
S2	66.2	14.4	19.4
S3	67.5	15.3	17.2
S4	73.0	11.6	15.4
S5	67.9	13.5	18.6
S6	70.6	12.8	16.6
S7	67.7	16.1	18.2

3.3 Soil Moisture Content Index

The soil moisture index (SMI) of the farm with an area of about 75,500 m^2, ranges from 0.184 to 0.385 as shown in Figure 7. SMI of 0.26 – 0.38 was classified as wet covering 25.7 % of the total farm area. 42.4 % of the farm has an SMI range of 0.21 to 0.26 and was classified as moist, while the remaining landmass of 31.9 % has SMI of 0.18 to 0.21, classified dry as shown in table 5. This implies that about 70% of the farm has SMI, ranging from moist to wet, making nutrients to be adequately mobilized for plant intake.

Table 5. Soil moisture content status in the study area

Soil moisture Index	Classification	Area (m^2)
0.18 – 0.21	Dry	24,100
0.21 – 0.26	Moist	32,000
0.26 – 0.38	Wet	19,400

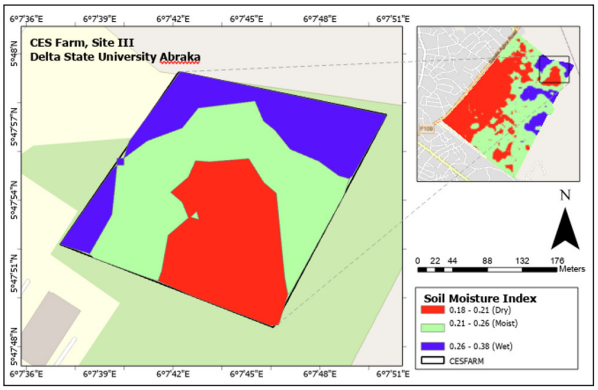

Figure 7. Soil Moisture index map of the CES farm, DELSU

3.4 Conclusion

Integrated geophysical methods and soil test analysis have been used to determine the nature of the soil in the CES farm Delta State University, Abraka, for its suitability in crop production. To maximize agricultural output while preserving soil and water resources, precise agriculture requires creating site-specific management techniques for crops based on the diversity of soil parameters. The soil of the research regions has been described, and management zones have been established, using geoelectrical resistivity imaging. The measurement of the soil fertility level of the farm was aided by a geochemical examination of earth samples and soil moisture content index from Landsat 8 imagery. The results showed that the soil is moderately rich in mineral content and organic matter required for crop production. The contamination factor and pollution index of the soil are quite low which is an indication that the soil is suitable for crop production.

Generally, determining what the soil requires to enhance crop growth is almost impossible without conducting soil analysis. Analyzing and testing soil helps understand its capacity to furnish adequate nutrients for supporting plant development and yield. Soil analysis also helps in determining the right combination of fertilizers and liming materials required for soil improvement. Therefore, with this study, using combined geophysical methods and soil test analysis in studying the evolution and pollution history of the soil have consistently demonstrated reliable results overtime.

Competing Interest Statement

In connection with this study, the authors have stated that they hold no financial or personal interests.

Data Availability Statement

All data generated by this study that supports its conclusions can be provided upon a formal request to the corresponding author.

Funding Declaration

The authors did not receive any funding from any organization for conducting this study.

Ethics Approval and Consent to Participate

Not Applicable

References

Aizebeokhai, A.P. (2010). 2D and 3D Geoelectric Resistivity Imaging: Theory and Field Design. Scientific Research and Essays 5 (23): 3592–3605.

Al-Amoush H, Abu Rajab J., Al-Tarazi E., Al-Shabeeb A.R., Al-Adamat R. Al-Fugara A. (2017). Electrical Resistivity Tomography Modeling of Vertical Lithological Contact using Different Electrode Configurations. Jordan Journal of Earth and Environmental Sciences 8(1): 27 – 34.

Al-Rashed M, Mukhopadhyay A., Al-Senafy A., Ghoneim, H. (2010). Contamination of Groundwater from Oil Field Water Disposal Pits in Kuwait. The Arabian Journal for Science and Engineering 35: 105 - 123

Ali A., Khaled H., Mostafa M., Abdulla A., Omar A., Mohammad Z., Amer M. (2022). Landsat/ MODIS Fusion for Soil Moisture Estimation over a Heterogeneous Area in Northern Jordan. Jordan Journal of Earth and Environmental Sciences 13 (4): 247-262.

Allred, B.J, Ehsani, M.R. Daniels, J.J. (2008). General considerations for Geophysical Methods Applied to Agriculture. Hand-Book of Agricultural Geophysics. 1st ed., CRC Press, Taylor and Francis Group, Boca Raton, Florida.

Altunay N., Hazer B., Tuzen M., Elik A. (2021). A New Analytical Approach for Preconcentration, Separation and Determination of Pb (II) And Cd (II) in Real Samples using a New Adsorbent: Synthesis, Characterization, and Application. Food Chemistry 359, 129923.

Anomohanran, O. (2015). Hydrogeophysical Investigation of Aquifer Properties and Lithological Strata in Abraka, Nigeria. Journal of African Earth Sciences 102: 247-253.

Aweto, K. E., Chiyem, F. I. and Ohwoghere-Asuma, O. (2017). Comparative Study of Total Dissolved Solids Evaluated from Resistivity Sounding, Water Analysis and Log Data. Scientia Africana 16(2): 38-43.

Briffa, J. Sinagra, E. and Blundell, R. (2020). Heavy Metal Pollution in the Environment and Their Toxicological Effects on Humans. Heliyon 6(9), e04691.

Carlson, T. N., Gillies, R. R., Perry, E. M. (1994). A Method to Make Use of Thermal Infrared Temperature and NDVI Measurements to Infer Surface Soil Water Content and Fractional Vegetation Cover. Remote Sensing Reviews 9(1-2): 161–173.

Chinyem, F.I. (2024). Determination of Aquifer Hydraulic Parameters and Groundwater Protective Capacity in Parts of Nsukwa Clan, Nigeria. Environmental Monitoring Assessment 196, 243.

Finch, F. Roldan, R. Walsh, L. Kelly, J., Amor, S. (2018). Analytical Methods for Chemical Analysis of Geological Materials, Government of New Foundland and Labrador, Department of Natural Resources. Department of Natural Resources, Geological Survey, Open File NFLD/3316.

Ganiyu, S.A. Olurin, O.T. Oladunjoye, M.A. Badmus, B.S. (2020). Investigation of Soil Moisture Content Over a Cultivated Farmland in Abeokuta Nigeria Using Electrical Resistivity Methods and Soil Analysis. Journal of King Saud University-Science 32 (1): 811–821.

Ijaz, M., Ahmad, H. R., Bibi, S., Ayub, M. A., Khalid, S. (2020). Soil Salinity Detection and Monitoring Using Landsat Data: A Case Study from Kot Addu, Pakistan. Arabian Journal of Geosciences 13(13): 510.

Iserhien-Emekeme, R.E., Ofomola, M.O., Ohwoghere-Asuma, O., Chinyem, F.I., Anomohanran, O. (2021). Modelling Aquifer Parameters Using Surficial Geophysical Techniques: A Case Study of Ovwian, Southern Nigeria. Modeling Earth Systems and Environment 7(4): 2297–2312.

Liu H, Cui H, Wang Y, Jiang Z, Lei L, Wei S. (2023). Accurate Determination of Trace Cadmium in Soil Samples with Graphite Furnace Atomic Absorption Spectrometry Using Metal-Organic Frameworks as Matrix Modifiers. Applied Spectroscopy 77(2):131-139.

Loke, M.H. (2010). Res2Dinv ver. 3.59 for Windows XP/ Vista/7, 2010. Rapid 2-D Resistivity & IP Inversion Using the Least-Squares Method. Geoelectrical Imaging 2D & 3D. Geotomo Software.

Lu, X. Zhang, X. Li, L.Y., Chen, H. (2014). Assessment of Metals Pollution and Health Risk in Dust from Nursery Schools in Xi'an, China. Environmental Research 128: 27–34.

Mashal K, Salahat M., Al-Qinna M, Ali Y. (2017). Assessment of Heavy Metals in Urban Areas of Al Hashmiyya City of Jordan. Jordan Journal of Earth and Environmental Sciences 8(2):61 - 67

Nemerow, N.L. (1991). Stream, Lake, Estuary and Ocean Pollution. 2nd ed., Van Nostrand Reinhold Publishing Company, New York.

Nowka, R., Marr, I.L., Ansari, T.M., Müller, H. (1999). Direct Analysis of Solid Samples by GFAAS – Determination of Trace Heavy Metals in Barytes. Fresenius' Journal of Analytical Chemistry 364: 533-540.

Ofomola, M. O, Akpolile, A.F, Anomohanran, O., Adeoye T.O, Bawallah, M.A. (2021). Detection of Trace Metal Contamination Around a Dumpsite in Iyara Area Warri Nigeria Using Geoelectrical and Geochemical Methods. Environmental and Earth Sciences Research Journal 8(3); 125-133.

Ofomola, M.O. (2015). Mapping of Aquifer Contamination Using Geoelectric Methods at a Municipal Solid Waste Disposal Site in Warri, Southern Nigeria. Journal of Applied Geology and Geophysics 3(3): 39 – 47.

Ofomola, M.O., Ako, B.D., Adelusi, A.O. (2016). Flow Direction and Velocity Determination of Dumpsite-Induced Groundwater Contamination in Part of Delta State, Nigeria. Arabian Journal of Geosciences 9, 398.

Ofomola, M.O., Iserhien-Emekeme, R.E., Okocha, F. O., Adeoye, T. O (2018). Evaluation of Subsoil Competence for Foundation Studies at Site III of the Delta State University, Nigeria. Journal of Geophysics and Engineering 15(3): 638–657.

Ozegin, K.O., Salufu S.O. (2022). Electrical Geophysical Method and GIS in Agricultural Crop Productivity in a Typical Sedimentary Environment. NRIAG Journal of Astronomy and Geophysics 11(1): 69-80.

Rashid, A., Schutte, B.J., Ulery, A., Deyholos, M.K., Sanogo, S., Lehnhoff, E.A., Beck, L. (2023). Heavy Metal Contamination in Agricultural Soil: Environmental Pollutants Affecting Crop Health. Agronomy 13(6), 1521.

Romero-Ruiz, A., Linde, N., Keller, T., Or, D. (2018). A Review of Geophysical Methods for Soil Structure Characterization. Reviews of Geophysics 56(4): 672-697.

Saikat M., Arka J. C., Abu M. T., Talha B. E., Firzan N., Ameer K., Abubakr M. I., Mayeen U. K., Hamid O., Fahad A. A., Jesus S. (2022). Impact of Heavy Metals on the Environment and Human Health: Novel Therapeutic Insights to Counter the Toxicity. Journal of King Saud University – Science 34, 101865

Tajudin, N., Ya'acob, N., Mohd Ali, D., Adnan, N. A. (2021). Soil Moisture Index Estimation from Landsat 8 Images for Prediction and Monitoring Landslide Occurrences in Ulu Kelang, Selangor, Malaysia. International Journal of Electrical and Computer Engineering 11(3): 2101-2108.

Tomlinson, D.C, Wilson, J.G, Harris, C.R, Jeffrey, D.W. (1980). Problems in The Assessment of Heavy Metals LevelsiIn Estuaries and The Formation of Pollution Index, Helgoland Marine Research 33 566–575.

Turki, N., Elaoud, A., Gabtni, H., Trabelsi, I., Khalfallah, K. K. (2019). Agricultural Soil Characterization Using 2D Electrical Resistivity Tomography (ERT) after Direct and Intermittent Digestate Application. Arabian Journal of Geosciences 12(14).

Vander-Velpen, B.P.A. (2004). WinRESIST (Version 1.0) Resistivity Depth Sounding Interpretation Software. M.Sc Research Project, ITC, Delft, the Netherland.

Vásconez-Maza, M. D., Bueso, M. C., Faz, A., Acosta, J. A., Martínez-Segura, M. A. (2021). Assessing the Behaviour of Heavy Metals in Abandoned Phosphogypsum Deposits Combining Electrical Resistivity Tomography and Multivariate Analysis. Journal of Environmental Management 278, 111517.

Verdoodt, A., Van Ranst, E. (2003). Land Evaluation for Agricultural Production in the Tropics. A Large-Scale Land Suitability Classification for Rwanda. Ghent University, Laboratory of Soil Science

WHO/FAO. (2001). Codex Alimentarius Commission. Food additives and contaminants. Joint FAO/WHO Food Standard Programme.